Secondary Flow and Upstream Dynamics in Double Bifurcation Model

Fong Yew Leong[a], Kenneth A. Smith[a,b], Chi-Hwa Wang[a,c]

[a] *Singapore-MIT Alliance,* [b] *Massachusetts Institute of Technology,* [c] *National University of Singapore*

***Abstract* – Flow behavior in bifurcation models is of great importance to health risk assessments and pulmonary drug delivery. This is particularly true of secondary flow behavior in multi-bifurcation models. Previously, both numerical and experimental methods have shown that four-vortex secondary flow structures can develop in the cross-sections of grand-daughter branches. This work shows that the development of secondary flow in the grand-daughter tubes is due to local stretching of vortex lines in the upstream DT. Scaling arguments have been used to derive two critical parameters governing this particular vorticity transport problem. A simple model for vorticity generation and transport is proposed, taking into account the geometric limitations imposed by the rigid walls of the tubes.**

Index Terms **– bifurcation, lung, secondary flow, vortex stretching**

I. Introduction

The secondary flows produced by bifurcations are of great importance to an understanding of aerosol transport to lung tissue and pulmonary drug delivery. Steady flow in single bifurcation models yields counter-rotating vortices in the daughter branches during the inspiratory phase [1]. These are qualitatively not unlike those commonly found in flow in curved tubes [2,3]. The complexity of the bifurcation geometry almost demands models to be based on computational fluid dynamics (CFD), although some insights can be gained from semi-analytical works involving a mother tube with circular cross-section bifurcating into semi-circular daughter tubes[4,5]. In human airways, the typical length-to-diameter ratios do not allow for fully developed flow profiles between bifurcations, as shown by Weibel's morphometric lung model [6].

Recent CFD efforts have revealed more complicated flow structures in symmetric double bifurcation models [7,8] and triple bifurcation models [9,10]. These symmetric bifurcation models may not be fully representative of actual lung casts, but are frequently popular for direct comparison of experimental and theoretical findings. There are also multi-bifurcation models based on physiologically realistic lung geometries [11,12]. These models may be more physiologically representative but they also tend to yield more complicated solutions which may mask the underlying physical phenomena.

Multi-bifurcation models have revealed complex secondary flows with multi-vortex configurations. In a double bifurcation model for instance, the prevalent secondary flow structure in the grand-daughter branches is shown to be a set of four counter-rotating vortices at high Reynolds numbers [11]. The additional set of counter-rotating vortices close to the inner walls of the grand-daughter branches are opposite in sense to those found in the case of the centrifugally-induced vortices observed in single bifurcation models. There is, however, a lack of detailed understanding in the development of these vortices in multi-bifurcation models despite the various numerical solutions to physiologically representative bifurcation models.

In addition to numerical simulations, there are a number of experimental studies which report the transient flow behavior of fluids in rigid single bifurcation models. Although these experimental models lack anatomical details of the human airways, they can be reliably reproduced for validation purposes [7]. Earlier works involve velocity measurements using the hot-wire probes and smoke tracers for flow visualization [13]. Flow visualization in single bifurcation models has earlier revealed not only the set of counter-rotating vortices in the secondary flow of the daughter branches, but also a characteristic double peaked axial velocity profile in the plane of the bifurcation and a characteristic M-shaped profile in the

This work is supported by the Singapore-MIT Alliance

Fong Yew Leong is with the Singapore-MIT Alliance, MEBCS Program, National University of Singapore, 4 Engineering Drive 3, Singapore 117576, Singapore

Kenneth A. Smith is with the Singapore-MIT Alliance and the Massachusetts Institute of Technology, 77 Massachusetts Ave Cambridge, MA 02139, USA

Chi-Hwa Wang is with the Singapore-MIT Alliance and the Department of Chemical and Biomolecular Engineering, National University of Singapore, 10 Kent Ridge Crescent, Singapore 119260, Singapore

plane perpendicular to the bifurcation. Modern measurement techniques have included Laser-Doppler Velocimetry (LDV) and Particle Image Velocimetry (PIV). These non-invasive optical techniques often yield good resolution on primary axial [14]. The difficulty posed by secondary flows is highlighted in [15], which cites diffraction losses and imaging depths as major sources of measurement errors. To the knowledge of the authors, there is as yet no reported experimental work on secondary flow in a double bifurcation.

As an illustrative double bifurcation model, here we present the dependence of the secondary flow behavior in the grand-daughter branches on the upstream conditions and the geometry of the carinal ridge. The problem is handled through both numerical and experimental approaches.

II. MATERIAL/VORTEX LINES

In general, the characteristic Re has to be much larger than unity in order to yield the four-vortex configuration in the grand-daughter tubes. It is therefore anticipated that the inviscid assumption will be valid except in the near-wall region. Therefore, the vortex line will always contain the same fluid particles. We can in fact exploit this classical feature by tracing the evolution of vortex lines connected by a single velocity streamline.

Starting with the RGDT of the double bifurcation model (Re 250), we first specify two reference positions corresponding to the vortex centers in the upper symmetrical half of an arbitrary cross section in the RGDT (one that intersects the carinal ridge is chosen for this study). We first trace a velocity streamline from the reference position at the inner vortex (one near the inner wall of the GDT), and several locus points are identified on the streamline. Vortex lines are now traced from those loci as shown in **Fig. 1**. These vortex line are in fact closed (as expected), and so for simplicity, they are termed as vortex rings (note the labels VR-A to VR-D). The color scheme refers to the dimensionless vorticity in the component parallel to the RGDT (positive in the direction towards the outlet). The top-down view is provided in **Fig. 1a**, and the side-view perspectives are shown in **Fig. 1b** and **Fig 1c**.

The upstream initial condition for the vortex ring is represented by VR-A which is a half-ring due to the symmetry condition at the MT. It carries null vorticity in the direction parallel to the RGDT but it is not irrotational. At VR-B, the half-ring from VR-A is joined by another half-ring near the wall. The original half-ring is noticeably extended in the direction of RGDT and the vortex ring becomes curved (**Fig. 1c**). The actual stretching in fact takes place at four localized regions on the vortex ring: two on each half-ring. This results in an intensification of vorticity in the component parallel to RGDT at those specific regions. At VR-C, the vortex ring has adopted a C-shaped form, which corresponds well with the commonly observed 'M-shaped' axial velocity profiles in single bifurcations. Just before the vortex ring reaches the carinal ridge at VR-D, the original half-ring now manifests as the inner vortices at the inner wall of RGDT (**Fig. 1c)**. In contrast, the other half-ring generated from the DT inner wall contributes to the formation of the outer vortices. Hence, we deduce that the basis for vortex formation in the GDT is already established in the upstream DT through the extension of the vortex lines.

Similar method has been used for the LGDT, starting from plotting velocity streamline from a specified reference point on the inner vortex core, followed by tracing four vortex rings from selected points on the streamline. These vortex rings, which are identified as VR-E, VR-F, VR-G and VR-H, are shown in the set of figures on **Fig. 2**. We observe similar qualitative features between the cases for LGDT and RGDT. An illustrative upstream initial condition is presented by VR-E, which is a half-ring due to the symmetry condition but carries finite vorticity in the direction parallel to the LGDT as the result of the fully developed entrance profile (in contrast with VR-A). The vortex ring VR-F is now a full ring, which curves inwards to a C-shaped VR-G. Finally, interaction with the carinal ridge deforms the vortex ring and it is now 'butterfly-shaped' (quad-lobed) as shown by VR-H. The extension of vortex line in the direction of the LGDT has resulted in an increased vorticity in the LGDT component at four localized regions **(Fig. 2b)**. This has led to the formation and observation of the four-vortex structure in the LGDT.

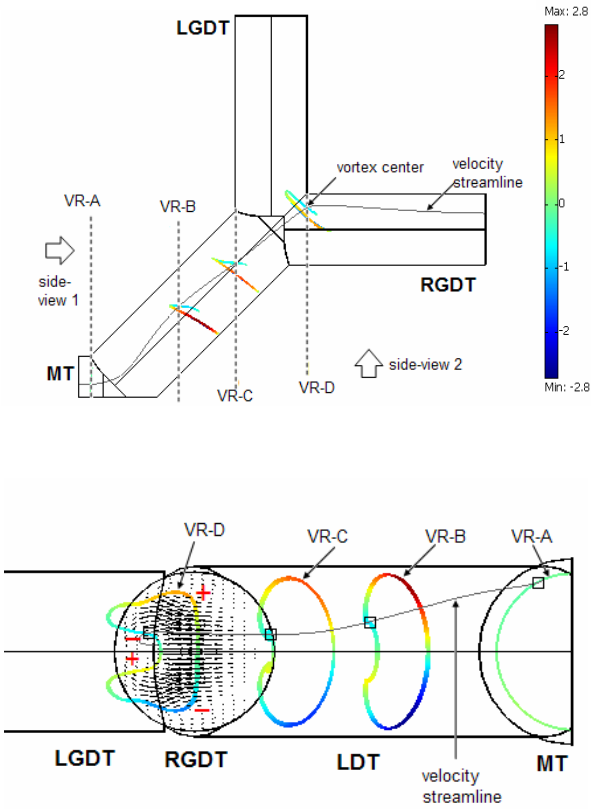

Fig. 1a (Top): Top-down view of double-bifurcation model (Re 250). Vortex rings linked by velocity streamline through inner vortex (RGDT). Color-bar shows dimensionless vorticity in RGDT component. Fig. 1b (Middle): Side-view 1; Fig. 1c (Bottom): Side-view 2

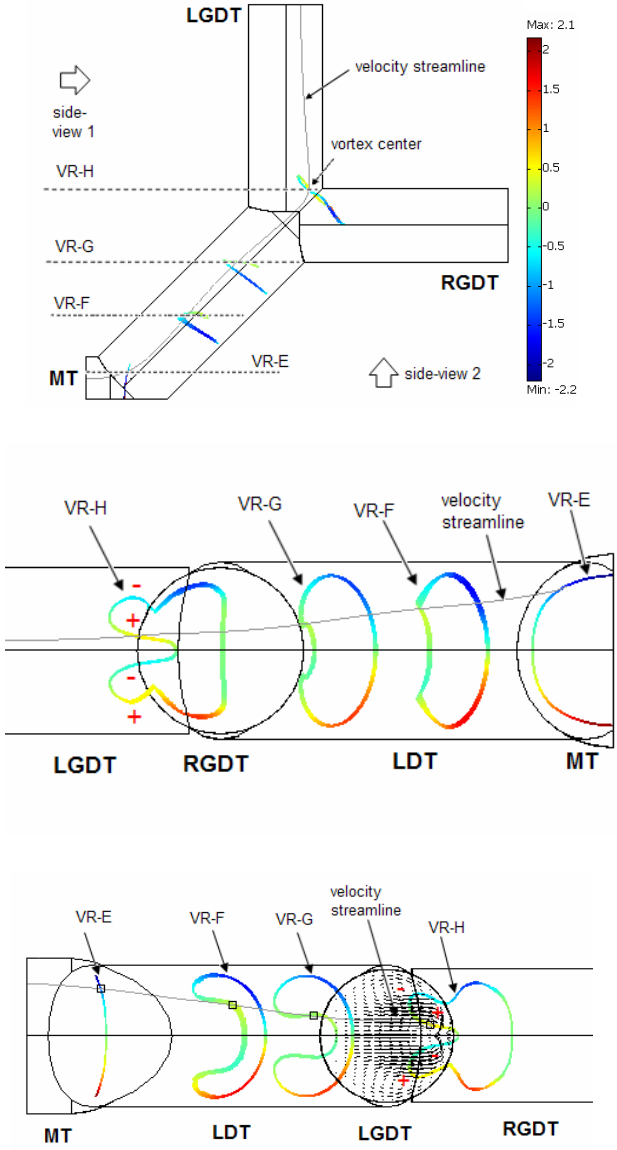

Fig. 2a (Top): Top-down view of double-bifurcation model (Re 250). Vortex rings linked by velocity streamline through inner vortex (LGDT). Color-bar shows dimensionless vorticity in LGDT component. Fig. 2b (Middle): Side-view 1; Fig. 2c (Bottom): Side-view 2

III. SCALING LAWS

The numerical simulation in the previous section has shown that localized extension of the vortex lines in the upstream daughter tube is responsible for the generation of vorticities in the grand-daughter tubes. This finding suggested that it may be possible to have a simple physical explanation for the secondary flow structures in the grand-daughter tubes.

We first begin with the vorticity transport equation.

$$\frac{\partial \overline{\omega}}{\partial t} + \overline{u} \cdot \nabla \overline{\omega} = \overline{\omega} \cdot \nabla \overline{u} + \nu \nabla^2 \overline{\omega} \qquad (1)$$

For steady state analysis, the temporal term on the left can be neglected, and that leaves us with the remaining three other terms to work on. Even though there are three scalar component equations of the vorticity transport vector equation (1), we can think of the flow as consisting of the main flow along of the axis of the tube (axial component) and the secondary flow perpendicular to the axis (secondary component), which are denoted as x and y respectively.

In this way, the convective term in the axial and secondary directions can be described respectively as

$$u\frac{\partial \omega_x}{\partial x} + v\frac{\partial \omega_x}{\partial y} \qquad u\frac{\partial \omega_y}{\partial x} + v\frac{\partial \omega_y}{\partial y} \qquad (2)$$

where u and v are the components of the velocity vector in the axial (x) and secondary (y) directions; and ω_x and ω_y are the respective components of the vorticity vector.

Similarly, the vortex stretching term can be written as

$$\omega_x\frac{\partial u}{\partial x} + \omega_y\frac{\partial u}{\partial y} \qquad \omega_x\frac{\partial v}{\partial x} + \omega_y\frac{\partial v}{\partial y} \qquad (3)$$

And finally, the viscous term can be written as

$$\nu\frac{\partial^2 \omega_x}{\partial x^2} \qquad \nu\frac{\partial^2 \omega_y}{\partial y^2} \qquad (4)$$

where ν is the kinematic viscosity of the fluid.

If we consider solely the axial component of the vorticity, we have estimates for the inertial term as

$$u\frac{\partial \omega_x}{\partial x} \sim \frac{U\Omega_x}{L} \qquad (5)$$

And the viscous term can be scaled as

$$\nu\frac{\partial^2 \omega_x}{\partial y^2} \sim \frac{\nu\Omega_x}{\delta^2} \qquad (6)$$

Where δ is an unspecified viscous length-scale (or boundary layer thickness)

It is worth noting that a bifurcation, in the absence of curvature, is no different from a straight tube. In other words, it is the centrifugal acceleration due to the curved bifurcation geometry that drives the secondary flow acting through the pressure gradient term in the momentum equations (which vanished as a term when the curl of the equation was taken). A representative term for the centrifugal acceleration would then be $\frac{u^2}{R}$, where R is the radius of curvature.

The secondary flow problem is now considered. Based on what has been observed in the numerical simulation previously, the vortex line (or ring) is distorted and stretched by the secondary flow as shown in the schematic diagram (**Fig. 3)**. This in turn leads to an increase in the vorticities along the vortex line with respect to the grand-daughter tubes (GDT).

Hence it is observed that in the absence of secondary flow, there can be no stretching of the vortex line in the cross-section of DT. In the case of the bifurcation geometry, the secondary flow is generated by the centrifugal acceleration, which is caused by the fluid having to negotiate a curvature. Hence, it is concluded that secondary flow is insignificant without centrifugal acceleration (it is assumed that displacement effect caused by new intervening wall surface at the carinal ridge is negligible).

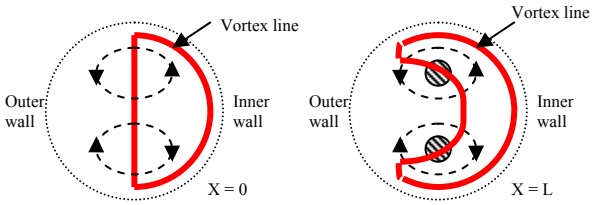

Fig. 3 (Left): Schematic Diagram of Vortex Line in Cross-section of DT. Fig. 3 (Right): Vortex Line at an arbitrary distance L downstream. Dashed lines refer to secondary flow streamlines. Bold red lines refer vortex lines. Shaded region refers to a local increase in secondary vorticity

Hence, we examine the secondary flow equation of motion and gather the order of magnitude estimates in the following manner:

$$\text{Convective: } u\frac{\partial v}{\partial x} \;\; v\frac{\partial v}{\partial y} \qquad \text{Estimate: } \frac{UV}{L} \;\; \frac{V^2}{a} \qquad (7)$$

$$\text{Centrifugal: } \frac{u^2}{R} \qquad \text{Estimate: } \frac{U^2}{R} \qquad (8)$$

$$\text{Viscous: } \nu\frac{\partial^2 v}{\partial y^2} \qquad \text{Estimate: } \frac{\nu V}{\delta^2} \qquad (9)$$

Since the scales for the convective and viscous terms (7 and 9) are functionally dependent on V, we start a hypothetical scaling argument about the centrifugal acceleration term.

- If the axial convective term is dominant, then

$$\frac{UV}{L} \sim \frac{U^2}{R} \Rightarrow \quad V \sim \frac{L}{R}U \qquad (10)$$

This would require the axial convective term to be dominant over both the radial convective term and the viscous term. In other words, the following inequalities must be satisfied, using the scaling for V determined in (10).

$$\frac{UV}{L} >> \frac{V^2}{a} \Rightarrow \quad \left(\frac{L}{a}\right)^2\left(\frac{a}{R}\right) << 1 \qquad (11)$$

$$\frac{UV}{L} >> \frac{\nu V}{\delta^2} \Rightarrow \quad \left(\frac{U\delta}{\nu}\right)\left(\frac{\delta}{L}\right) >> 1 \qquad (12)$$

- If the secondary convective term is dominant, then

$$\frac{V^2}{L} \sim \frac{U^2}{R} \Rightarrow \quad V \sim \left(\frac{a}{R}\right)^{1/2}U \qquad (13)$$

This would require the secondary convective term to be dominant over both the axial convective term and the viscous term. The following inequalities must be satisfied, using the scaling for V determined in (13).

$$\frac{V^2}{a} >> \frac{UV}{L} \Rightarrow \quad \left(\frac{L}{a}\right)\left(\frac{a}{R}\right)^{1/2} >> 1 \qquad (14)$$

$$\frac{V^2}{a} >> \frac{\nu V}{\delta^2} \Rightarrow \quad \left(\frac{a}{R}\right)^{1/2}\left(\frac{U\delta}{\nu}\right)\left(\frac{\delta}{a}\right) >> 1 \qquad (15)$$

- Lastly, if the secondary viscous term is dominant,

$$\frac{\nu V}{\delta^2} \sim \frac{U^2}{R} \Rightarrow \quad V \sim \left(\frac{U\delta}{\nu}\right)\left(\frac{\delta}{R}\right)U \qquad (16)$$

Similarly, this would require the viscous term to be dominant over both the convective terms, in the spirit of the boundary layer theory. The following inequalities must be satisfied, using the scaling for V determined in (16).

$$\frac{\nu V}{\delta^2} >> \frac{UV}{L} \Rightarrow \quad \left(\frac{U\delta}{\nu}\right)\left(\frac{\delta}{L}\right) << 1 \qquad (17)$$

$$\frac{\nu V}{\delta^2} >> \frac{V^2}{a} \Rightarrow \quad \left(\frac{U\delta}{\nu}\right)^2\left(\frac{\delta}{R}\right)\left(\frac{\delta}{a}\right) << 1 \qquad (18)$$

Based on the inequalities specified above, two key parameters are identified, namely $\left(\frac{U\delta}{\nu}\right)\left(\frac{\delta}{L}\right)$ and $\left(\frac{L}{a}\right)\left(\frac{a}{R}\right)^{1/2}$, which are used to scale the secondary flow. This allows us to define three separate transport regimes (axial convective, radial convective and viscous).

Hence, the scaling argument for the vorticity equation is exactly identical to the equation of motion (since all the terms scale by a constant). The corollary to this observation is that, even though the scale for V depends on the dominance of respective terms in the equation of motion, it does not affect the dominance of the respective terms in the vorticity transport equation.

Based on the two parameters as identified earlier, namely $\left(\frac{U\delta}{\nu}\right)\left(\frac{\delta}{L}\right)$ and $\left(\frac{L}{a}\right)\left(\frac{a}{R}\right)^{1/2}$, a map of dominant regimes for the vorticity transport equation can be constructed as shown in **Fig. 4**.

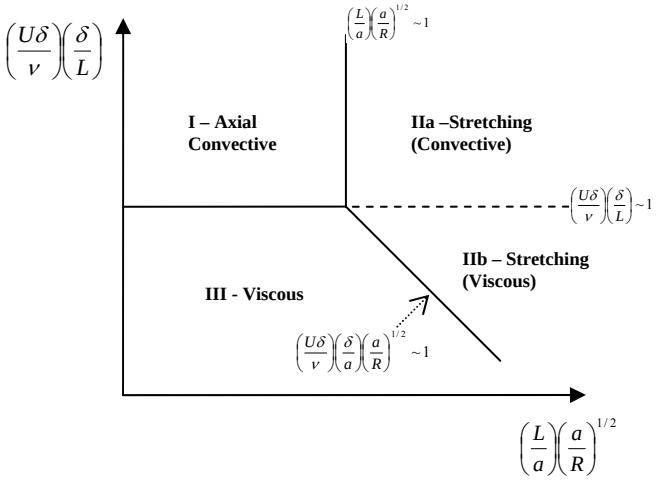

Fig. 4: Schematic Diagram of Flow Regimes Based on Scaling Arguments

IV. Vorticity Transport Modeling

Since the earlier scaling argument can only provide an order-of-magnitude description of the problem, we seek to improve the accuracy of the theoretical estimates. The following discussion is based on the premise that vortex stretching is the dominant source of secondary vorticity, or in other words, $\left(\frac{L}{a}\right)\left(\frac{a}{R}\right)^{1/2} >> 1$.

With that in mind, hypothetical transport models with varying geometrical assumptions are proposed.

We shall begin from the solution of the simplest case without the vortex stretching term (i.e. pure convective-diffusive transport) before moving on to other cases which involves the analysis of the vortex stretching term.

Case One: Pure Convective-Diffusive Transport

It is assumed that the generation of secondary vorticity occurs instantaneously over a very short time-scale, so that the secondary vorticity generation profile resembles a Dirac delta. This allows us to neglect the vortex stretching term from the vorticity transport equation (since the bulk of the transport is convective-

diffusive). The simplification is substantial because vorticity only enters the problem as a transportable scalar quantity to be specified as an initial condition.

For a two-dimensional case as depicted in **Fig. 5**, we are examining fluid flow at relatively high Reynolds numbers between a pair of parallel plates, which corresponds to the upper and lower walls of the daughter tube. The coordinates of interest here are the horizontal x and the vertical z. The assumed uniform velocity condition far upstream (x < 0) encounters a sudden curvature at the entrance (x = 0) and then straightens out for a distance of 0 < x < L. It is assumed that the fluid instantaneously attains an unknown quantity of secondary vorticity, which we set as $\Omega_y(z)$ for the initial vorticity condition (the subscript y is the out of plane vector orthogonal to x and z). The increase in vorticity in this two-dimensional problem modifies the velocity gradient so the velocity profile deforms as shown in **Fig. 5**, where the vorticity on the symmetrical top and bottom halves are opposite in directions. As the fluid moves towards the outlet (x = L), the outward diffusion of vorticity causes the velocity gradient to decay. The preceding description of the problem resembles strongly the case of the wake of the flow past a flat plate.

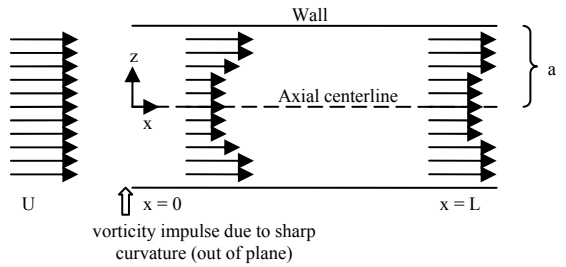

Fig. 5: Schematic Diagram of Flow Between Two Parallel Plates With Specified Upstream Vorticity

We define velocity difference as

$$\wedge(x,z) \equiv U - u(x,z) \qquad (19)$$

It is assumed that $\wedge << U$, which at low vorticity magnitudes, may in fact be easier to satisfy in this present problem than for the case of wake past a flat plate. The reason is that the centerline velocity at the origin does not have to be zero, as is the case for a flat plate (due to the enforced no-slip condition).

Taking the curl of the momentum equation and simplifying, we obtain

$$U\frac{\partial \omega_y}{\partial x} = \nu\frac{\partial^2 \omega_y}{\partial z^2} \qquad (20)$$

The boundary conditions for the secondary vorticity ω_y are

$$\omega_y(x,0) = 0 \qquad (21)$$

$$\omega_y(x,a) = 0 \qquad (22)$$

$$\omega_y(0,z) = \Omega_y(z) \qquad (23)$$

The first boundary condition (21) is based on the condition of null shear stress at the plane of symmetry (z = 0). The second boundary condition (22) requires the assumption that the boundary layer thickness of the upper wall is thin ($\delta_v << a$), so that the stationary point of the velocity profile ($\partial u/\partial z = 0$) is positioned at $z \cong a$, where $0 \le z \le a$. The last boundary condition (23) is an entrance condition and also the upper limit of the vorticity without further vortex stretching.

With the boundary conditions (21-23), the boundary value problem is now fully specified and sufficiently simple to solve by a variety of analytical methods. The confined dimensional specification of the problem suggests that the similarity method is not the best method, so instead the Finite Fourier Transform (FFT) method is used. Detailed solution is provided in Appendix A.

The solution obtained is

$$\overline{\omega}_y(x,z) = \sqrt{2}\sum_{n=1}^{\infty}\Omega_{yn}\exp\left(-\frac{(n\pi)^2\,\overline{x}}{\mathrm{Re}_a}\left(\frac{L}{a}\right)\right)\sin n\pi\overline{z} \qquad (24)$$

$$\Omega_{yn} = \omega_{yn}(0) = \int_0^1\left(\sqrt{2}\sin n\pi\overline{z}\right)\Omega_y(\overline{z})\,d\overline{z}$$

where the variables on overbars indicate that they have been rendered dimensionless via $\overline{\omega}_y = \omega_y(a/U)$, $\overline{x} = x/L$ and $\overline{z} = z/a$

We first draw our attention to the exponential factor. It basically tells us that

- The parameter of importance in the axial transport of vorticity is $\mathrm{Re}_a^{-1}\left(\frac{L}{a}\right)$. This is certainly related to the boundary layer parameter $\left(\frac{U\delta}{\nu}\right)\left(\frac{\delta}{L}\right)$ that we have obtained earlier in the derivation of the scaling laws for the case of $\delta = a$.

- Secondary vorticity decays almost exponentially with downstream axial distance. This result provides an insight into how the vorticity quantity is transported and was not obtained directly in the previous scaling arguments. It may be helpful in the comparison with numerically obtained values.

Case Two: Generation of Secondary Vorticity and Convective Transport

In the attempt to resolve the convective-diffusive development of secondary by analytical means, the generation of secondary vorticity in Case One had been neglected.

How is secondary vorticity generated in the daughter tube? It is known that the pair of counter-rotating vortical secondary flow structure found in daughter tubes is mainly caused by the centrifugal acceleration of the fluid having to negotiate a segment of finite curvature. Even though these vortices are predominantly axial in direction, the fluid shear distorts and extends the vortex lines along the cross-sectional plane, thus increases the secondary vorticity by stretching (see **Fig. 6**). As suggested in the earlier scaling arguments, it is assumed that the secondary vorticities should scale similarly to the secondary flow (due to the similarity between the secondary equation of motion and the vorticity transport equation).

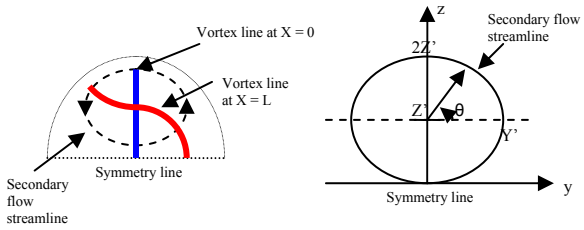

Fig. 6: Schematic Diagram of Vortex Lines in Cross-section of DT (Left) and the characteristic secondary flow streamline (Right)

Close examination of the scaled secondary flow parameter $\left(\frac{L}{a}\right)\left(\frac{a}{R}\right)^{1/2}$ suggests that it is not sufficient to use this parameter directly in the analysis of the secondary vorticity. Instead, it is noted that the cross-sectional geometry of the daughter tube can in fact impose a physical constraint on the growth of the secondary vorticity. More specifically, the vortex line cannot possibly stretch indefinitely in any secondary direction, due to the no-penetration condition of the side walls.

It appears to be impossible to obtain an exact solution to the vortex stretching process without solving the full momentum equations. Instead, we propose a simplified working model.

A schematic diagram of the upper symmetrical half of the cylinder cross-section is as shown in **Fig. 6**. In this model, several assumptions are made. First of all, a characteristic secondary flow streamline is defined with the center positioned at the center of the upper half of the cross-section, or a distance of $Z' = a/2$, where a is the radius of the tube. The characteristic minor semi-axis of the ellipse is Z' and the characteristic major semi-axis is Y', where $Y' = \sqrt{2}Z' = \sqrt{2}a/2$.

The characteristic angular velocity along the secondary flow streamline is defined as V, which we can relate to our previous scaling argument. We assume that secondary convection due to centrifugal acceleration is significant, so that the scale for secondary velocity is defined as $V \sim \left(\frac{a}{R}\right)^{1/2} U$ (13), where R is the radius of curvature and U is the characteristic axial velocity.

We are interested in the stretching of vortex line in the y-component, hence we start by resolving the secondary velocity in the y-component. The ellipse as shown in **Fig. 6 (Right)** can be expressed in polar coordinates as

$$\begin{aligned} y &= -Y'\sin\theta \\ z &= Z'(1+\cos\theta) \end{aligned} \qquad (25)$$

We shall restrict our analysis to a parametric angle of $0 \le \theta \le \pi/2$ **(Fig. 6 Right).** The time scale parameter is defined as $t \sim x/U$ where x is the axial component. The derivative of y with respect to time t (in subscripts) is written as

$$y_t = -Y'\cos\theta \cdot \theta_t \qquad (26)$$

Now the angular velocity can be expressed as a function of the secondary velocity $\theta_t = \frac{V}{r}$

Since $r = \sqrt{y^2 + (z - Z')^2}$, eqn (26) can be written as a function of time t only:

$$\begin{aligned} \left|\frac{y_t}{V}\right| &= \frac{Y'\cos\theta}{\sqrt{y^2 + (z - Z')^2}} \\ &= \sqrt{\frac{(Y'\cos\theta)^2}{(Y'\sin\theta)^2 + (Z'\cos\theta)^2}} \\ &= \left((\tan\theta)^2 + \left(\frac{Z'}{Y'}\right)^2\right)^{-1/2} \end{aligned} \qquad (27)$$

Where $\theta = \int_0^t \frac{V}{r}\,dt$

From eqn (27), we verify that

$$\left|\frac{y_t}{V}\right| \to \left(\frac{Y'}{Z'}\right) \qquad \text{as} \qquad \theta \to 0 \qquad (28)$$

$$\left|\frac{y_t}{V}\right| \to 0 \qquad \text{as} \qquad \theta \to \pi/2 \qquad (29)$$

What the above limits tells us is that the rate of vortex extension starts off at the theoretical maximum as indicated in (28) and decreases to zero as the trigonometric limiting term becomes significant as indicated in (29). This is important because it is indicative of the limitations of the generation of secondary vorticity via vortex stretching.

With the assumed secondary velocity scale of $V \sim \left(\frac{a}{R}\right)^{1/2} U$, we generalize an estimation of the vortex stretching term as

$$\left|\frac{y_t}{a}\right| \sim \left[(aR)\left((\tan\theta)^2 + \left(\frac{Z'}{Y'}\right)^2\right)\right]^{-1/2} U \qquad (30)$$

For this assumed case with negligible viscous effects, we can simplify the vorticity transport equation in the same way as was shown in **Case 1**.

$$\frac{\partial \omega_y}{\partial x} \approx \left[(aR)\left((\tan\theta)^2 + \left(\frac{Z'}{Y'}\right)^2\right)\right]^{-1/2} (\omega_y) \qquad (31)$$

We assume that the radius of curvature depends weakly on x. For the case of $\theta \to 0$ which occurs near the bifurcation point $x \to 0$, eqn (31) simplifies to

$$\frac{\partial \ln \omega_y}{\partial x}\Big|_{x\to 0} \approx \frac{1}{\sqrt{aR}}\frac{Y'}{Z'} \qquad (32)$$

which implies exponential dependence of the secondary vorticity on early axial distance.

On the other hand, for $\theta \to \pi/2$ which occurs at some unknown axial distance x = L', eqn (32) simplifies to

$$\frac{\partial \omega_y}{\partial x}\Big|_{x\to L'} \to 0 \qquad (33)$$

Hence, we recognize that in the absence of viscous effects, a plot of secondary vorticity as a function of axial distance in fact suggests a sigmoidal trend, i.e. an early exponential growth followed by decreasing growth rates and eventually a stationary point.

Subsequently, at larger values of axial distance x, vorticity generation due to vortex stretching becomes insignificant and the viscous effects become dominant. In this case we revert to the earlier presented results for **Case 1**.

V. Numerical Analysis

Numerical study has been conducted for an incompressible fluid flow in a planar double bifurcation model with a variable length-to-diameter ratio in the DT. The objective is to analyze the effects of the axial length-scale on vorticity transport and verify the hypothesized vorticity transport model. All other geometric parameters are held constant, e.g. the bifurcation angles for both first and second bifurcations are set at 90º. Boundary conditions are fully developed flow at the inlet, no-slip condition at the walls and null pressure condition at the outlets.

Numerical simulations are conducted under quasi-steady conditions for a range of Re up to 336, using a sinusoidal varying velocity input. A total of 20 different sets of double bifurcation models are examined, each differing from one another only by the length of the DT, measured from bifurcation center to bifurcation center. Numerical convergence for each case required approximately 24 hours, and the number of finite elements used ranges from approximately 40,000 to 80,000. With the converged solution field, a cross-section is taken from LGDT and RGDT as shown in **Fig. 7**, each one provided an allowance of a fixed distance of 1.5a from the second bifurcation axis (where a is the radius of the MT and the characteristic length-scale of the problem). We shall define a length parameter here as dimensionless axial distance, which is the sum of the length of DT and the fixed distance, normalized by the characteristic length a.

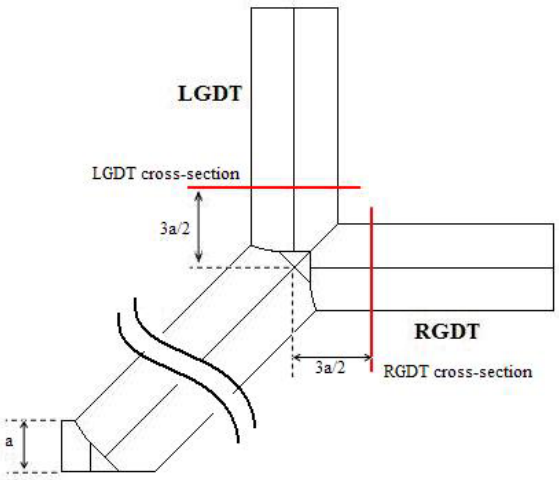

Fig. 7: Schematic Diagram of Double Bifurcation Model (Symmetrical about centerline of MT) – Length of DT is varied in each simulation run

In each cross-section, the vorticity field in the direction of the respective GDT can be derived. Thus the maximum point vorticity magnitudes can be identified by inspection. Since the objective of this study is to analyze the vorticity due to the stretching of vortex

lines in the fluid core, the near-wall vorticities magnitudes are neglected. In each cross-section under inspection, either two or four distinct regions of elevated vorticity magnitudes can be identified.

Only the vorticity component in the direction of each respective GDT is considered. For convenience, this variable is loosely termed as 'streamwise vorticity' in the subsequent analysis, even though the local primary velocity may not exactly parallel to the respectively GDT. This streamwise vorticity ω_{GDT} is rendered dimensionless via $\overline{\omega}_{GDT} = \frac{\omega_{GDT} \cdot a}{U}$, where a is the radius of MT and U is the centerline velocity of the MT.

Fig. 8 shows the variation of the averaged maximum streamwise vorticity magnitudes for the four different vortex regions under the effect of varying dimensionless axial distance, at an instantaneous Re of 336.

We observe that the profiles for the inner and outer vorticities are distinctive and different. The outer vorticity for the RGDT increases sharply for small values of dimensionless axial distance, and subsequently declines with increasing values of that parameter. On the other hand, the outer vorticity for the LGDT increases monotonically with increasing distance within the range covered by this study. The inner vorticity profiles for both GDT are qualitatively similar, with an increase in magnitude, until the axial distance of about 4 is reached, and later decays with increasing axial distance. Also note the cross-over intersecting point between the LGDT vorticities at an axial distance of approximately 6.2.

Since only the inner vorticities originate from the DT fluid core and are accompanied by stretching of the vortex line, we will be looking at these in greater detail. In the schematic shown in Fig. C earlier, the early increase in vorticities is hypothesized to be exponential in the form of eqn (32), which can be expressed as

$$\omega_y \sim \exp\left(\frac{Y'}{Z'}\sqrt{\frac{a}{R}}\right)\bar{x} \qquad (34)$$

Where Y' and Z' are the major and minor semi-axes of the hypothetical ellipse as shown in Fig. 4.2 (Right), a is the radius of MT, R is the radius of curvature and x is axial distance. We assume that the actual profile is indeed exponential as predicted and regression of the initial data points both inner vortex curves reveals an average exponential value of about 2.6 (as shown in **Fig. 8**). Then, matching the regression profile and eqn (34), and assuming a value of 1.5 for the ratio of the semi-axes (Y'/Z') of the hypothetical ellipse, the estimate for the curvature ratio (a/R) is about 0.33, which seems to be a reasonable figure.

From eqn (33)

$$\frac{\partial \overline{\omega}_y}{\partial \bar{x}}\Big|_{\bar{x}\to L'} \to 0 \qquad (35)$$

There is not much to be done about eqn (35), since it only predicts a stationary point in the vorticity profile, and it is already observed to be the case as shown in **Fig. 8**.

From eqn (24)

$$\overline{\omega}_y(\bar{x},\bar{z}) = \sqrt{2}\sum_{n=1}^{\infty}\Omega_{yn}\exp\left(-\frac{(n\pi)^2\bar{x}}{\mathrm{Re}_a}\right)\sin n\pi\bar{z} \qquad (36)$$

The final eqn (36) suggests an exponential decline of the vorticity with increasing axial distance. The first term Regression of the terminal data points of both inner vortex curves reveals exponential values of -0.33 and -0.49 for the RGDT and LGDT respectively. This is approximately one order of magnitude higher than the predicted value of ~0.04. This suggests that vorticity decay may not be the only explanation for the decline of vorticity at large axial lengths.

Reverting to the vorticity transport equation, it appears probable that the explanation for the observed phenomenon is the presence of a non-trivial vortex *destretching* term. Unlike vortex stretching, it is not immediately clear how the destretching process can occur. It is speculated that viscous decay of the secondary flow velocity results in a negative acceleration in the secondary direction. Unfortunately, the inclusion of the vortex stretching term makes the vorticity transport equation highly non-linear, so this particular issue has not been resolved as yet.

Location		**Vorticity origin (DT)**	**Positive vorticity (towards outlet)**	**Negative vorticity (away from outlet)**
RGDT	Inner	Core	Lower half cross-section	Upper half cross-section
RGDT	Outer	Near-wall	Upper half cross-section	Lower half cross-section
LGDT	Inner	Core	Upper half cross-section	Lower half cross-section
LGDT	Outer	Near-wall	Lower half cross-section	Upper half cross-section

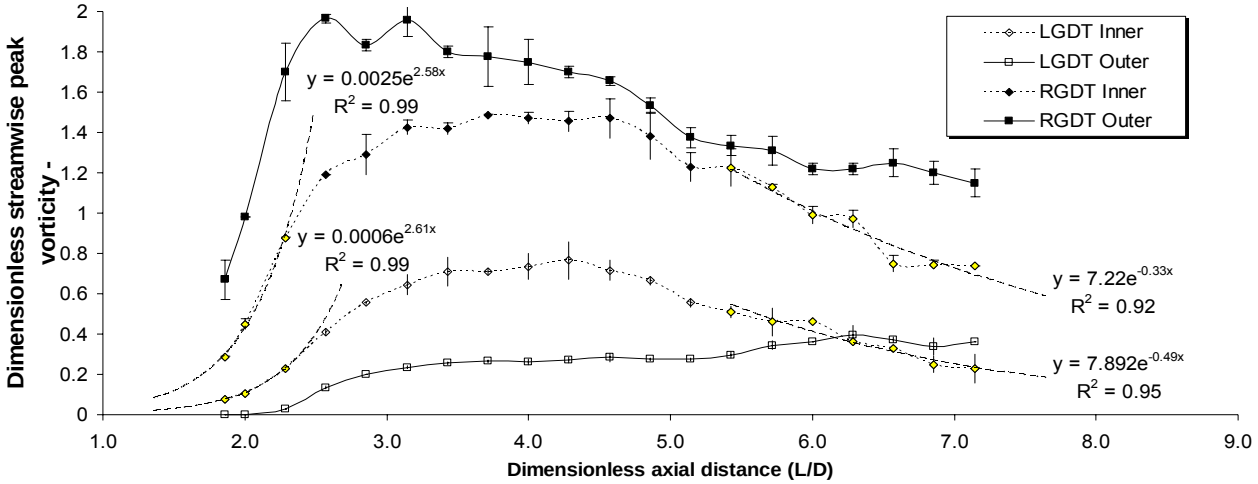

Fig. 8: Dimensionless streamwise maximum vorticity as a function of dimensionless axial distance at Re 336

VI. CONCLUSION

We have demonstrated strong evidence of vortex stretching phenomena in the upstream DT leading up to the formation of 4-vortex configuration in the secondary flow of GDT downstream. Scaling arguments have been used to derive two critical parameters governing this particular vorticity transport problem. A simple model for vorticity generation and transport is proposed, taking into account the geometric limitations imposed by the rigid walls of the tubes. Numerical computation of streamwise vorticity profiles shows reasonable agreement with theory at low length to diameter ratios. Inaccuracy at higher length to diameter ratios suggests possible vortex destretching due to viscous decay.

Acknowledgement

The authors would like to thank Mr Lim Wee Chuan for suggestions and comments.

Reference

[1] Pedley T.J. The Fluid Mechanics of Large Blood Vessels. Cambridge University Press. 1980

[2] Dean W.R., Fluid in a curved channel. Proc. R. Soc. London, Ser. A, 121, 402, 1928.

[3] Olson D.E., Fluid mechanics relevant to respiration: flow within curved or elliptical tubes and bifurcating systems. PhD Thesis, Imperial College, London, 1971.

[4] Tadjfar M. and F.T. Smith, Direct simulations and modeling of basic three-dimensional bifurcating tube flows. J. Fluid Mech. 519, 1-32, 2004.

[5] Blyth M.G. and A.J. Mestel, Steady flow in a dividing pipe. J. Fluid Mech. 401, 339-364, 1999.

[6] Weibel E.R. Morphometry of the human lung. Academic Press, New York. 1963.

[7] Comer C.K., C. Kleinstreuer, Z. Zhang, Flow structures and particle deposition patterns in a double-bifurcation airway models. 1. Air flow fields. J Fluid Mech. 435, 25–54, 2001.

[8] Calay R.K., J. Kurujareon, A.E. Holdo, Numerical simulation of respiratory flow patterns within human lung. Respiratory Physio. Neurobiology 130, 201-221, 2002.

[9] Zhang Z. and C. Kleinstreuer, Transient airflow structures and particle transport in a sequentially branching airway model. Phys. Fluids. 14, 862–880, 2002.

[10] Zhang Z., C. Kleinstreuer, C.S. Kim, Flow structure and particle transport in a triple bifurcation airway model. J. Fluids Eng. 123, 320–330, 2001.

[11] Ertbruggen C., C. Hirsch, M. Paiva, Abatomically based three-dimensional model of airways to simulate flow and particle transport using computational fluid dynamics. J. Appl. Physio. 98, 970-980, 2005.

[12] Nowak N., P.P. Kakade, A.V. Annapragada, Computational fluid dynamics simulation of airflow and aerosol deposition in human lungs. Ann. Biomed. Eng., 31, 374-390, 2003.

[13] Schroter R.C. and M.F. Sudlow, Flow patterns in models of the human bronchial airways. Respir. Physiol. 7, 341–355, 1969.

[14] Brücker C.H. and M.L. Riethmuller, Cyclic flow oscillations in a system of repeatedly branching channels. Phys. Fluids 10(4), 877-885, 1998.

[15] Fresconi F.E., A.S. Wexler, A.K. Prasad, Expiration flow in a symmetric bifurcation. Experiment in Fluids 35, 493-501, 2003.

Appendix A: Convective-diffusive transport of secondary vorticity

This section entails the solution of eqn (4.2) using Finite Fourier Transform (FFT). We first non-dimensionalize the problem by normalizing the length variables x with respect to L and z with respect to a, and the secondary vorticity with respect to (U/a). For simplicity, we shall use the same notation for the dimensionless variables in this section as before.

The problem statement for $\omega_y(x,z)$ is

$$\frac{\partial \omega_y}{\partial x} = G\frac{\partial^2 \omega_y}{\partial z^2} \tag{A-1}$$

$$\omega_y(x,0) = 0 \tag{A-2}$$

$$\omega_y(x,1) = 0 \tag{A-3}$$

$$\omega_y(0,z) = \Omega_y(z) \tag{A-4}$$

where $G = \mathrm{Re}_a^{-1}\left(\frac{L}{a}\right)$

Assuming that the solution can be written in the form of a series expansion,

$$\omega_y(x,z) = \sum_{n=1}^{\infty} \omega_{yn}(x)\Phi_n(z) \tag{A-5}$$

$$\Phi_n(z) = \sqrt{2}\sin n\pi z,\ n = 1,2,... \tag{A-6}$$

where $\Phi_n(z)$ is the basis function.

The transformed vorticity is defined as

$$\omega_{yn}(x) = \int_0^1 \Phi_n(z)\omega_y(x,z)dz \tag{A-7}$$

We apply FFT to both sides of (A-1), to give

$$\int_0^1 \Phi_n(z)\left[\frac{\partial \omega_y}{\partial x} - G\frac{\partial^2 \omega_y}{\partial z^2}\right]dz = 0 \tag{A-8}$$

The first term is simply

$$\int_0^1 \Phi_n(z)\frac{\partial \omega_y}{\partial x}dz = \frac{d\omega_{yn}}{dx} \tag{A-9}$$

Whereas the second term requires integration by parts,

$$\begin{aligned}
&\int_0^1 \Phi_n(z)\frac{\partial^2 \omega_y}{\partial z^2}dz = \Phi_n\frac{\partial \omega_y}{\partial z}\bigg|_{z=0}^{z=1} - \int_0^1 \frac{d\Phi_n}{dz}\frac{\partial \omega_y}{\partial z}dz \\
&= \Phi_n\frac{\partial \omega_y}{\partial z}\bigg|_{z=0}^{z=1} - \left(\omega_y\frac{d\Phi_n}{dz}\bigg|_{z=0}^{z=1} - \int_0^1 \omega_y\frac{d^2\Phi_n}{dz^2}dz\right) \\
&= \left(\Phi_n\frac{\partial \omega_y}{\partial z} - \omega_y\frac{d\Phi_n}{dz}\right)\bigg|_{z=0}^{z=1} - (n\pi)^2\omega_{yn}
\end{aligned} \tag{A-10}$$

We have defined our basis function such that $\Phi_n(0) = \Phi_n(1) = 0$, and referring to (A-2) and (A-3) boundary condition, the transformed equation (A-8) becomes

$$\frac{d\omega_{yn}}{dx} + G(n\pi)^2\omega_{yn} = 0 \tag{A-11}$$

Applying the last boundary condition (A-4), the solution is then

$$\omega_{yn} = \Omega_{yn}e^{-G(n\pi)^2 x} \tag{A-12}$$

where Ω_{yn} is a constant evaluated as

$$\Omega_{yn} = \omega_{yn}(0) = \int_0^1 \Phi_n(z)\Omega_y(z)dz \tag{A-13}$$

Substitute (A-12) in (A-5) yields the general solution

$$\omega_y(x,z) = \sqrt{2}\sum_{n=1}^{\infty}\Omega_{yn}e^{-G(n\pi)^2 x}\sin n\pi z \tag{A-14}$$

Incidentally, if Ω_y is a constant, (A-14) can be written as

$$\omega_y(x,z) = 2\Omega_y\sum_{n=1}^{\infty}\frac{\left(1-(-1)^n\right)}{n\pi}e^{-G(n\pi)^2 x}\sin n\pi z \tag{A-15}$$